International Journal of Solids and Structures 50 (2013) 2857–2871

Contents lists available at SciVerse ScienceDirect

International Journal of Solids and Structures

journal homepage: www.elsevier.com/locate/ijsolstr

An efficient modelling of inelastic composites with misaligned short fibres

D. Notta-Cuvier *, F. Lauro, B. Bennani, R. Balieu

Université Lille Nord de France, F-59000 Lille, France
UVHC, LAMIH, UMR CNRS 8201, Le Mont-Houy, F-59313 Valenciennes, Cedex 9, France

ARTICLE INFO

Article history:
Received 25 September 2012
Received in revised form 29 March 2013
Available online 15 May 2013

Keywords:
Short fibre reinforced composites
Misaligned fibres
Distributed orientation

ABSTRACT

This paper deals with the modelling of the behaviour of short-fibre reinforced composites. The composite is seen as an assembly of a matrix medium and of several fibre media. Each fibre medium, characterised by its own orientation of fibres and volume fraction, is considered as a one-dimensional elastic medium. The matrix material has an elastoplastic behaviour. All types of hardening laws can be considered, thanks to a valuable adaptivity of the modelling. The use of the Drucker–Prager criterion for plasticity and non-associative plasticity rules allow to deal with compressible plastic flow. Moreover, all kind of orientation of fibres, in particular random orientations and imperfect alignments, can be modelled in a simple way. The influence of the fibres' orientation on the mechanical response of a polymer matrix composite subjected to tensile/compression tests is analysed in detail. Finally, simulated behaviours of composites are compared to experimental data found in the literature.

1. Introduction

The material reinforcement with short fibres can be very effective thanks to the high rigidities of the fibres (e.g. about 70–80 GPa for glass fibres, more than 200 GPa for carbon fibres). The reinforcement consists in the dilution in a matrix material of a precise amount of fibres. Contrary to spherical inclusions, e.g., the aspect ratio of the fibres is well above 1. Actually, typical dimensions of short fibres are about 10–15 μm in diameter for lengths from 200 to 500 μm (i.e., aspect ratio from 13 to 50). It is therefore obvious that the composite's macroscopic behaviour can become fully anisotropic and that it strongly depends on the density and the orientation of the short fibres. Contrary to long fibres (continuous reinforcement), the orientation of short fibres is not so easy to control in the formation of composites, even injection moulded ones. It is now commonly accepted that fibres are actually oriented following a distribution of orientation that depends on the production process and on the density of the fibres. The local anisotropy of injection moulded fibre reinforced polymer composites can be studied using micro-tomography analyses (Bernasconi et al., 2008). Some authors have developed models to compute the orientation of fibres in injection moulded reinforced composites (Vincent et al., 1997; Doghri and Tinel, 2006).

Behaviour modelling of short fibre reinforced materials may be based on different approaches which are more or less complex. In the framework of linear elasticity, numerous studies demonstrate the relevance of simple macroscopic rules of mixture to predict the tensile/flexural apparent rigidity of composite materials, thanks to the linear constitutive laws. Originally, the rule of mixture between the matrix's rigidity and that of the fibres only considered the relative volume fraction of each constituent. Then, Bowyer and Bader, 1972 enriched the rule of mixture with corrective parameters that allow to take into account the distributions of fibres in terms of length and of orientation. Although the required expression of the shear stress transfer can be challenging (e.g. Detassis et al., 1995; Thomason, 2002), this simple approach gives rise to satisfactory results (e.g. Fu and Lauke, 1996; Thomason, 2001; Bernasconi and Cosmi, 2011) and can be adapted to various cases. For example, the rule can be enriched with a clustering parameter which is relevant when dealing with natural fibre reinforcements (Facca et al., 2007). However, the use of short-fibre reinforced materials in industrial applications makes it essential to understand and predict their response to more complex loadings, at higher levels of strain and/or strain rates,... In particular, the development of a plastic (or viscoplastic) flow in the material, and perhaps damage phenomena, must be dealt with. Obviously, such strongly non-linear and 3-dimensional behaviours can not be modelled with simple rules of mixture.

More elaborate modellings consider the composite material as a two-phase medium {matrix + fibres}. The way the phases are defined and linked to each other constitute the greatest divergences between approaches found in the literature. Some studies consider the composite as an assembly of representative elementary volumes (REV, or meso-regions) containing both phases. Drozdov et al. (2005) consider that the meso-regions are incompressible linear

* Corresponding author at: UVHC, LAMIH, UMR CNRS 8201, Le Mont-Houy, F-59313 Valenciennes, Cedex 9, France. Tel.: +33 685738743.
E-mail address: delphine.notta@univ-valenciennes.fr (D. Notta-Cuvier).

0020-7683/$ - see front matter © 2013 Elsevier Ltd. All rights reserved.
http://dx.doi.org/10.1016/j.ijsolstr.2013.04.031

elastic media. The plastic flow in the composite material is therefore assumed to be due to the slide of meso-regions with respect to each other. Drozdov et al. (2003) use the same hypotheses in the framework of viscoelasticity and viscoplasticity. However, although effective for the presented cases, such an approach seems difficult to extend to complex matrix behaviour, in particular to the case of a compressible medium.

In other approaches, finite element computations are used to solve the mechanical behaviour of each REV. The macroscopic behaviour is then modelled by the integration in the total material volume of the mechanical quantities computed for each REV, weighted if necessary by a function of fibres' orientation distribution (Levy and Papazian, 1991; Lorca et al., 1991; Modniks et al., 2011; Böhm et al., 2002). This method can however be costly because finite element models may require very fine meshes.

An increasingly widespread approach, which does not need finite element simulation, consists in treating the two-phase material as an inclusion-type problem, based on the theory originally developed by Eshelby (1957). Eshelby's theory is limited to materials containing very small volume fractions of inclusions because it only considers the local modifications of the strain and stress fields of the matrix, without taking interactions between inclusion phases into account. Significant improvements to Eshelby's theory are due to Mori and Tanaka (1973). In particular, their theory makes it possible to model the local interaction between inclusion phases because the matrix is seen as a medium perturbed by the other heterogeneities. Moreover, Eshelby's problem has an exact solution when dealing with linear elasticity but it has no analytical solution when the material has a non-linear behaviour. To overcome this difficulty, the non-linear behaviour of the individual components can be linearised so that an approximate solution based on the original Eshelby solution can be found (e.g. in elastoplasticity Hill, 1965 or in viscoplasticity Lebensohn and Tomé, 1993). An important point is that only average data within phases is obtained. Fluctuation of mechanical fields within homogeneous phases can be analysed with second-order moment approaches (e.g. for non-linear rigid viscoplastic materials Ponte-Castañeda, 2002). Approximate solution can however be improved using self-consistent or Mori–Tanaka schemes (Lagoudas et al., 1991; Mercier and Molinari, 2009; Schjødt-Thomsen and Pyrz, 2001; Doghri and Ouaar, 2003). The inclusion-type problems can become very difficult to state in the case of reinforcements with non-aligned short fibres (i.e., when fibres are not all aligned in the same direction). To overcome this difficulty, Doghri and Tinel (2005) developed a procedure of homogenisation in two steps. The first one is the homogenization of a two-phase "pseudo-grain" constituted of the matrix material reinforced with identical and aligned fibres; the second one consists in the homogenization of all pseudo-grains to compute the mechanical properties at the RVE scale. Recently, Kammoun et al. (2011) have improved the two-step procedure of homogenization to take damage phenomena into account in the second step.

All these contributions show that the difficulty of implementing such procedures of homogenisation, and even multi-homogenisation, increases significantly as the behaviour to model and the fibres' orientation distribution become more complex. It is therefore interesting to develop models of composite behaviours at an intermediate scale between these complex approaches and purely phenomenological description. An interesting theory is based on the multiplicative split of the deformation gradient tensor combined with the assumption of potentials (elastic, plastic, viscoelastic ..., as relevant) for each constituent. The composite is thus seen as the superposition of a matrix material and of several families of fibres. The deformation gradient that is applied to the composite as a whole and its multiplicative decomposition links the media implicitly. Klinkel et al. (2005) show it can be theoretically applied to non-linear elasto-plastic behaviours for the matrix and the fibres. Nevertheless, there is no concrete application of their implementation in the analysis of the behaviour of a short fibre reinforced material. Nedjar (2007) uses this approach for viscoelastic materials, assuming that fibres carry load only in tension. Again, the numerical results are not compared to experimental data.

Based on this approach, an effective modelling of short fibre reinforced composite materials is presented. The composite material is seen as an assembly of a matrix medium and several embedded fibre media. The modelling can deal with all types of rate-independent elastoplastic behaviours of the matrix. The Drucker–Prager pressure-sensitive criterion for plasticity is used, in the framework of non-associative plasticity. It allows to model compressible or incompressible plastic flow, as well as different behaviours under compression than under tension. It is essential to improve the modelling of polymer matrix composites, in particular. In addition, the modelling can be adapted to all types of hardening law with no need to modify the core of the numerical scheme, as exposed in Section 2.1. This adaptability can be of great interest for the characterisation of the unknown behaviour of a novel composite material.

Fibres that have the same mechanical properties and orientation are grouped into the same "family". Since fibres are assumed to carry load only in their direction of orientation, each medium of fibres is assumed to behave as a one-dimensional media. It is worth noticing that the distribution of the short fibres into several families allows to model all types of fibres orientation, including distributed and random orientations, in a simple way. The fibres' behaviour remains linear elastic. Indeed, it is very likely that the composite fails before the stress applied to the fibres reaches their initial yield stress, because of a ductile damage of the matrix material and/or fibres debonding, for example. So, extending the implementation to irreversible fibres behaviours is not relevant as long as these phenomena are not taken into account.

As described in Section 2, the mechanical behaviour is solved separately for each medium before composite's behaviour is established using an additive decomposition of the elastoplastic potential. An orientation tensor is used to relate the fibre orientation distribution with the anisotropic response of the composite. In Section 3, the influence of fibres orientation on the mechanical response of a polymer matrix composite (Drucker–Prager criterion) under tension and compression is analysed in detail, using numerically simulated tests. In Section 4, the results of the modelling are compared to experimental data found in the literature. The case of a metal matrix composite with randomly oriented short metallic fibres is first studied. The response of a polymer matrix composite with misaligned glass fibres subjected to tensile tests at different loading angles is then analysed.

2. Behaviour of inelastic materials reinforced with misaligned short fibres

The reinforced composite material is formed of short fibres assumed to be uniformly dispersed in an elastoplastic matrix. Each fibre is characterised by its orientation vector expressed in the global system of coordinates (i.e., linked to the composite or equivalently to the matrix). Fibres that have the same material behaviour and vector of orientation, $\vec{a}^i$, are grouped into family number i. In this way, n_{fam} families of fibres are considered. Each of them is characterised by a volume fraction, v_F^i, so that $\sum_{i=1}^{n_{fam}} v_F^i = v_F = 1 - v_M$. v_F and v_M are respectively the total volume fraction of fibres and matrix in the composite material.

When the composite material is subjected to loading, its deformation can be described by the tensor of deformation gradient, $\bar{F} = grad_X(x)$, where X and x are respectively the coordinates in

previous and current configurations. Here, the fundamental assumption is that the fibres carry loads only in their direction of orientation. Therefore, the tensor of deformation gradient that is actually applied to the family of fibres number i, $\bar{F}_F^i$, is the projection of the global tensor of deformation gradient along the fibres' orientation (1). The matrix is assumed to be subjected to tensor $\bar{F}$ in totality.

$$\bar{F}_F^i = \bar{F}A^i \ \forall i \in \{1, \ldots, n_{fam}\} \tag{1}$$

where A^i is the matrix of orientation of fibres' family i, defined by $A^i = \vec{a}^i \otimes \vec{a}^i$, i.e. $A^i_{kl} = a^i_k a^i_l, \ \forall k, l$ (no summation).

It is assumed that fibres behaviour remains linear elastic throughout the transformation whereas the matrix has an elastoplastic behaviour. Both behaviours are numerically determined before the stress state of the composite material is computed thanks to an additive decomposition of the specific free energy potential. The following paragraph presents the key points of the modelling of the elastoplastic behaviour of the matrix (more details can be found in Appendix). Then, the computation of the fibres behaviour and of the composite material as a whole are presented.

2.1. Elastoplastic behaviour of the matrix

The elastoplastic behaviour of the matrix material is described under the hypothesis of small deformations. A Drucker–Prager criterion (2) for plasticity is used. Contrary to the more widespread criterion of von Mises (J_2-plasticity), Drucker–Prager's criterion is pressure sensitive and is consequently often used to model the behaviour of polymer materials in particular:

$$\sigma_{eq} = J_2 + \eta\sigma_H \tag{2}$$

In the absence of kinematic hardening, J_2 is the von Mises equivalent stress, defined by $J_2 = \sqrt{\frac{3}{2}\bar{S} : \bar{S}}$, with $\bar{S}$ the deviatoric part of the Cauchy stress tensor of the matrix material, $\bar{\sigma}_M$. $\sigma_H = \frac{1}{3}tr(\bar{\sigma}_M)$ is the hydrostatic pressure and η is a material parameter. The introduction of the parameter ξ in the expression of the yield surface (3) allows to model a different yield stress in compression ($\sigma_C < 0$) than in traction (σ_T). The expressions of η and ξ are given by Eqs. (4) and (5), respectively (cf Appendix). σ_y is the yield stress whose evolution is governed by the hardening law, $R(p)$, identified in the case of a tensile loading (6). p is the cumulated plastic strain (expression given in Appendix):

$$f = J_2 + \eta\sigma_H - \xi\sigma_y \leqslant 0 \tag{3}$$

$$\eta = 3\frac{\sigma_T + \sigma_C}{\sigma_C - \sigma_T} \tag{4}$$

$$\xi = 1 + \frac{\eta}{3} \tag{5}$$

$$\sigma_y = \sigma_T + R(p) \tag{6}$$

The framework of non associative plasticity is considered. The plastic potential is expressed in a pressure sensitive form (7) in order to model a compressible behaviour of the matrix material. γ is a material parameter whose expression depends on the material but also on the nature of the loading. Indeed, the phenomena that govern the compressibility of a material, e.g. the growth of porosities, are influenced by the stress triaxiality. In particular, γ can be different in tension (positive hydrostatic stress) than in compression (negative hydrostatic stress) (cf Section 3). In the current model, γ is assumed to be a function of the plastic Poisson coefficient, ν_p, defined as the ratio $|\frac{\varepsilon_{II}}{\varepsilon_I}|$, where ε_I and ε_{II} are the two most important principal strains ($|\varepsilon_I| \geqslant |\varepsilon_{II}|$). ν_p provides information on the variation of material volume during the plastic flow, that can be significant when considering polymer materials, in particular. If the plastic deformation is isochoric, as for the vast majority of metallic materials, ν_p remains equal to 0.5. In practice, the value of ν_p is material dependent. It must be characterised experimentally (e.g. measures of volumetric strains):

$$\psi = J_2 + \gamma\sigma_H \tag{7}$$

The implementation of these constitutive laws is described in details in Appendix. It is worth noting that a subroutine is used in the preamble of the implementation to build a table that links the values of the cumulated plastic strain to those of the yield stress, according to the hardening law. A change of the hardening law therefore only affects this subroutine and not the core of the numerical scheme, thereby giving the model a valuable adaptivity.

2.2. Linear elastic behaviour of the fibres

As already stated, the presence of fibres in the composite material is modelled by the coexistence of n_{fam} families. In each family i ($i \in \{1, \ldots, n_{fam}\}$), all the fibres have the same elastic behaviour, the same vector of orientation, $\vec{a}^i$, and therefore the same matrix of orientation $A^i = \vec{a}^i \otimes \vec{a}^i$. $\vec{a}^i$ and A^i are assumed to remain constant during the loading. A volume fraction, v_F^i, is associated to each family, so that $\sum_{i=1}^{n_{fam}} v_F^i = 1 - v_M$, with v_M the volume fraction of the matrix material. From now on, the exponent i will be omitted to simplify the notations. In practice the implementation presented hereafter is obviously iterated for each family of fibres.

The aspect ratio (length divided by diameter) of short fibres used for reinforcement is generally not less than 15 (Bernasconi and Cosmi, 2011). It can therefore be assumed that fibres deform longitudinally while keeping a constant diameter, i.e. their deformation remains null in transverse directions. In other words, fibres are assumed to carry loads only in their axis direction, $\vec{a}$, and each family of fibres is assumed to behave like a one-dimensional medium. The tensor of deformation gradient that actually affects the fibres, $\bar{F}_F$, is the projection of the tensor of total deformation gradient, $\bar{F}$, in the direction of the fibres' orientation (1). Then, the right Cauchy–Green tensors, $\bar{C}$ and $\bar{C}_F$, defined by Eq. (8) are linked by the simple relation (9) (A is symmetric by construction):

$$\bar{C} = \bar{F}^T\bar{F} \quad \text{and} \quad \bar{C}_F = \bar{F}_F^T\bar{F}_F \tag{8}$$

$$\bar{C}_F = A\bar{C}A \tag{9}$$

By construction, $\bar{C}_F$ has a unique eigenvalue different from zero, called λ_F, that is coherent with a unidimensional behaviour of fibres media. The associated eigenvector is $\vec{a}$. λ_F actually stands for the square of the ratio of the fibres current length by initial length. As a consequence, the 1D Hencky strain of the fibres, ε_F, is simply expressed from λ_F, as stated by Eq. (10) (small strain hypothesis):

$$\varepsilon_F = \frac{1}{2}\ln(\lambda_F) \tag{10}$$

The fibres axial stress, σ_F, is then simply given by $\sigma_F = E_F\varepsilon_F$, with E_F the Young modulus of the fibres.

This formulation is actually consistent with a local iso-strain state between the fibres and the matrix, in the direction of the fibres axis. Yet, without correction this formulation can lead to unrealistic stress states and rigidities when applying the final "law of mixture" (described in the next section) for composites having highly angled fibres with respect to the loading direction. In particular, the axial stress computed for a composite material subjected to tensile loading transversally to the fibres direction would be equal to the matrix axial stress times the matrix volume fraction. As a consequence, the composite material would be less stiff than the neat matrix material. To prevent this unrealistic phenomenon, iso-stress states are assumed between the fibres and the matrix material in transverse and shear directions with respect to the fibres axis, that leads to

Table 1
Matrix material parameters.

Parameter	Value
Young modulus, E_M	2.1 GPa
Poisson coefficient, ν_M	0.3
Initial yield stress under tension, σ_T	29 MPa
Initial yield stress under compression, σ_C	−40 MPa
Hardening modulus (linear part), k_1	139 MPa
Hardening modulus (exponential part), k_2	32.7 MPa
Hardening coefficient, m	319.4
Plastic Poisson coefficient, ν_p	0.1 if $\sigma_H \geqslant 0$, 0.5 else

the expression (11) for the fibres stress tensor in the global system of coordinates, $\bar{\sigma}_F$. $\bar{\sigma}^0_M$ is the matrix stress tensor expressed in the fibres system of coordinates, defined by vectors $\vec{a}$, $\vec{a}^\perp$ and $\vec{a}\wedge\vec{a}^\perp$, with $\vec{a}\cdot\vec{a}^\perp = 0$. $\bar{\sigma}^0_M$ is therefore equal to $V^{-1}\bar{\sigma}_M V$. V is the transition matrix which columns are the vectors $\vec{a}$, $\vec{a}^\perp$ and $\vec{a}\wedge\vec{a}^\perp$. The axial stresses computed this way for composites subjected to transverse loadings with respect to the fibres orientation are equal to those of the matrix material, which is consistent with the well-known principle of lower bound assumption:

$$\bar{\sigma}_F = V\begin{bmatrix} \sigma_F & \sigma^0_{M12} & \sigma^0_{M13} \\ \sigma^0_{M12} & \sigma^0_{M22} & \sigma^0_{M23} \\ \sigma^0_{M13} & \sigma^0_{M23} & \sigma^0_{M33} \end{bmatrix} V^{-1} \tag{11}$$

2.3. Stress tensor applied to the composite material

After the computation of stress states for the matrix material and all the families of fibres, the stress tensor applied to the composite material can be determined. First, the state potential of the composite material is assumed to be split into a part specific to the matrix and other parts specific to each family of fibres (12).

$$\rho\Phi = v_M\rho_M\Phi_M + \sum_{i=1}^{n_{fam}} v^i_F\rho^i_F\Phi^i_F \tag{12}$$

with ρ, ρ_M and ρ^i_F the densities of the composite, of the matrix and of the family of fibres number i, respectively. This expression of Φ is used in the Clausius–Duhem inequality, here simplified for isothermal transformations (13).

$$\begin{aligned} &\bar{\sigma} : \bar{D} - \rho\frac{d\Phi}{dt} \geqslant 0 \\ &(12) \Rightarrow \bar{\sigma} : \bar{D} - \left[v_M\rho_M\frac{d\Phi_M}{dt} + \sum_{i=1}^{n_{fam}} v^i_F\rho^i_F\frac{d\Phi^i_F}{dt}\right] \geqslant 0 \end{aligned} \tag{13}$$

with $\bar{D}$ the tensor of rate of deformation that can be assimilated to $\dot{\bar{\varepsilon}}$ under the hypothesis of small perturbations. As defined in the framework of elastoplasticity for small perturbations and of isothermal transformations, Φ_M is a function of $\bar{\varepsilon}$, $\bar{\varepsilon}^e$, $\bar{\varepsilon}^p$ and p. $\bar{\varepsilon}^e$ and $\bar{\varepsilon}^p$ are actually redundant state variables if considering the strain partition $\bar{\varepsilon} = \bar{\varepsilon}^e + \bar{\varepsilon}^p$. The time derivative of Φ_M can therefore be expressed using the following partial derivative form:

$$\frac{d\Phi_M}{dt} = \frac{\partial\Phi_M}{\partial\bar{\varepsilon}} : \frac{\partial\bar{\varepsilon}}{\partial t} + \frac{\partial\Phi_M}{\partial\bar{\varepsilon}^p} : \frac{\partial\bar{\varepsilon}^p}{\partial t} + \frac{\partial\Phi_M}{\partial p}\cdot\frac{\partial p}{\partial t} \tag{14}$$

Each potential Φ^i_F is a function of the scalar ε^i_F, computed using Eq. (10). Yet, for convenience, the Hencky strain tensors expressed in the global system of coordinates by $\varepsilon^i_{Fkl} = V^i_{k1}V^{i-1}_{1l}\varepsilon^i_F$, $\forall k,l$, $\forall i$ are considered. So, $\frac{d\Phi^i_F}{dt} = \frac{\partial\Phi^i_F}{\partial\bar{\varepsilon}^i_F} : \frac{\partial\bar{\varepsilon}^i_F}{\partial t}$, $\forall i$. If assuming small displacements,

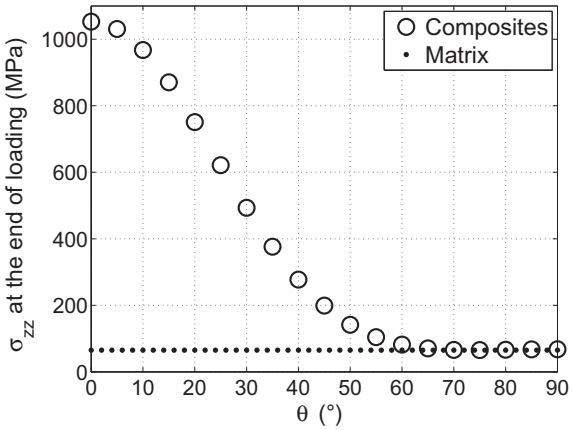

Fig. 2. Axial stress of composites at the end of tensile loading.

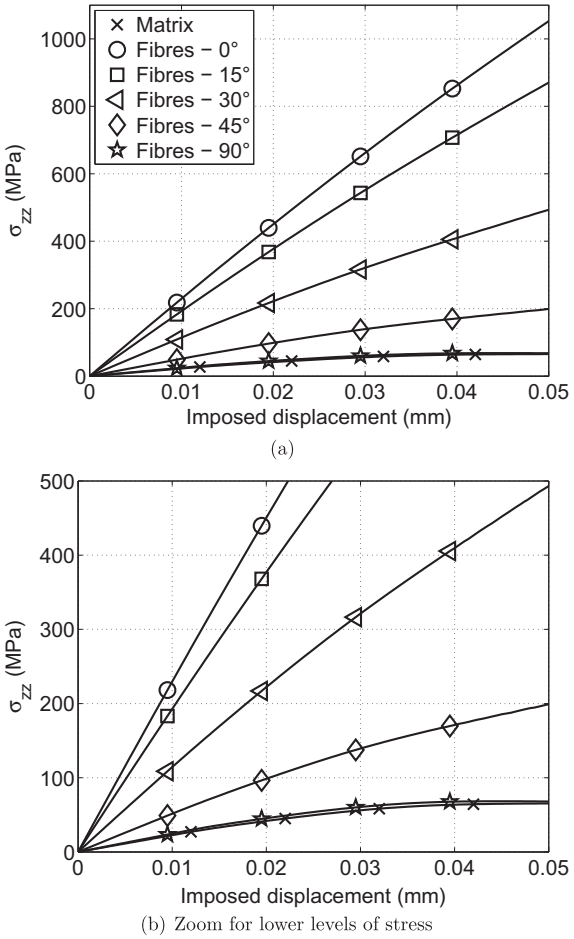

Fig. 3. Axial stress time histories for different composites PA-30% GF under tension.

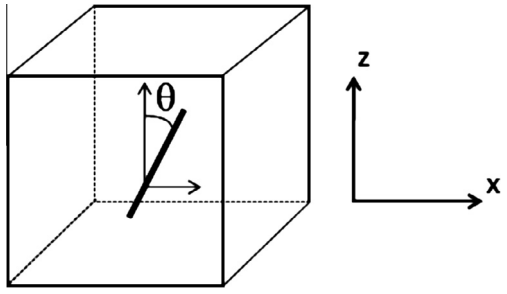

Fig. 1. Angle of orientation of short fibres.

the Hencky strain tensors can be assimilated to the Green–Lagrange strain tensors relative to the families of fibres, $\bar{E}_F^i$, that are expressed from the right Cauchy–Green tensors with $\bar{E}_F^i = \frac{1}{2}(\bar{C}_F^i - \bar{I}),\ \forall i$. So, the relation (9) leads to the approximation $\frac{\partial \bar{e}_F^i}{\partial t} \approx A^i \frac{\partial \bar{e}}{\partial t} A^i,\ \forall i$. Finally, these developments give rise to the factorized expression (15) for the Clausius–Duhem inequality, noting that $\bar{X} : \left(A^i \bar{Y} A^i\right) = \left(A^i \bar{X} A^i\right) : \bar{Y}$, for any tensors $\bar{X}$ and $\bar{Y}$, by construction of matrices A^i:

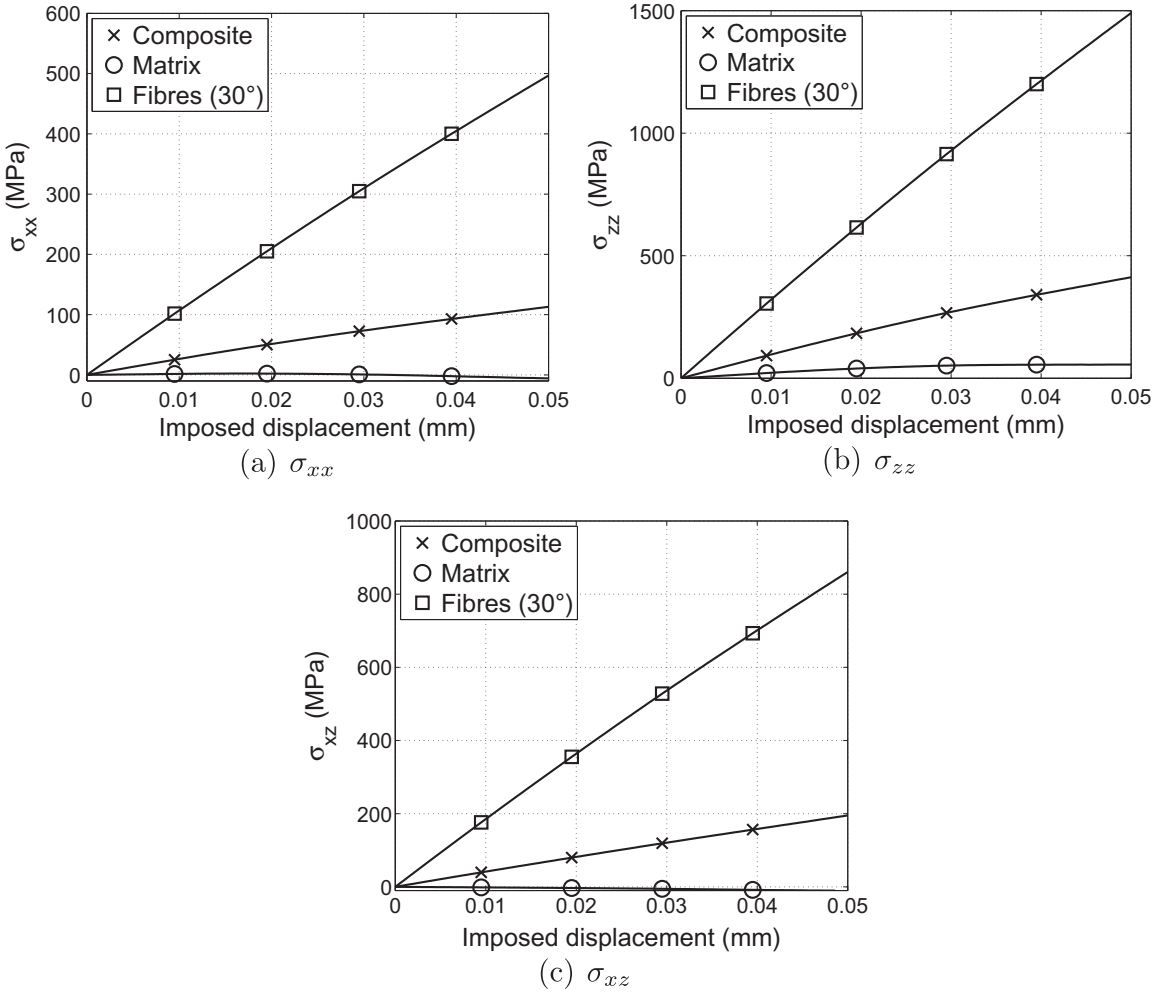

Fig. 4. Stresses under tension for the 30%vol. GF composite, the matrix material and the fibres ($\theta = 30^\circ$).

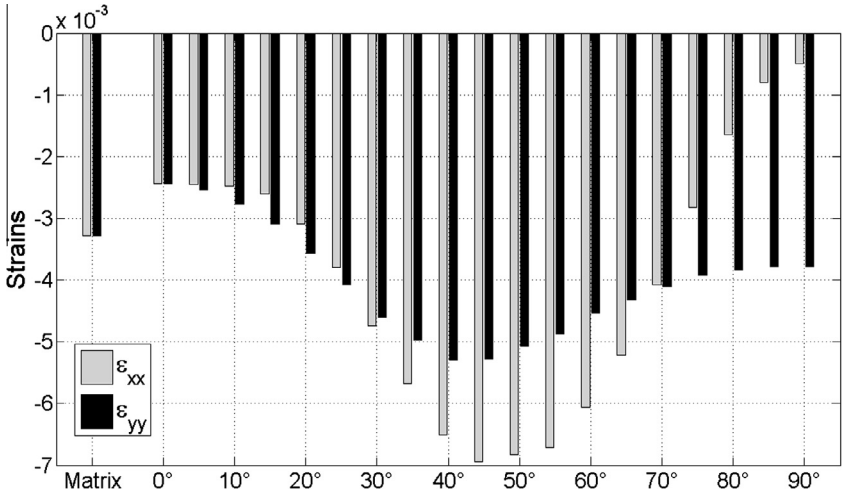

Fig. 5. Transverse strains of the composite materials – tension.

$$\mathcal{D} = \left[\bar{\sigma} - v_M \rho_M \frac{\partial \Phi_M}{\partial \bar{\varepsilon}} - \sum_{i=1}^{n_{fam}} v_F^i \rho_F^i A^i \frac{\partial \Phi_F^i}{\partial \bar{\varepsilon}_F^i} A^i\right] : \dot{\bar{\varepsilon}} - v_M \rho_M \left[\frac{\partial \Phi_M}{\partial \bar{\varepsilon}^p} : \left(\frac{\partial \bar{\varepsilon}^p}{\partial t} - \frac{\partial \bar{\varepsilon}^e}{\partial t}\right) + \frac{\partial \Phi_M}{\partial p} \cdot \frac{\partial p}{\partial t}\right] \geqslant 0 \quad (15)$$

Since the Clausius–Duhem inequality (15) has to be verified for any value of $\dot{\bar{\varepsilon}}$, the system $\mathcal{E}$ (16) is an admissible solution. Finally, considering the state laws $\rho_M \frac{\partial \Phi_M}{\partial \bar{\varepsilon}} = \bar{\sigma}_M$ and $\rho_F^i \frac{\partial \Phi_F}{\partial \bar{\varepsilon}_F^i} = \bar{\sigma}_F^i$, $\forall i$, the stress state of the composite material can be expressed in a simple form (17).

$$(\mathcal{E}) \begin{cases} \bar{\sigma} = v_M \rho_M \frac{\partial \Phi_M}{\partial \bar{\varepsilon}} + \sum_{i=1}^{n_{fam}} v_F^i \rho_F^i A^i \frac{\partial \Phi_F^i}{\partial \bar{\varepsilon}_F^i} A^i \\ -\frac{\partial \Phi_M}{\partial \bar{\varepsilon}^p} : \left(\frac{\partial \bar{\varepsilon}^p}{\partial t} - \frac{\partial \bar{\varepsilon}^e}{\partial t}\right) - v_M \rho_M \frac{\partial \Phi_M}{\partial p} \cdot \frac{\partial p}{\partial t} \geqslant 0 \end{cases} \quad (16)$$

$$\bar{\sigma} = v_M \bar{\sigma}_M + \sum_{i=1}^{n_{fam}} v_F^i A^i \bar{\sigma}_F^i A^i \quad (17)$$

3. Examples of numerical application

In this paragraph, the behaviour of a polymer matrix reinforced with short glass fibres subjected to uniaxial tensile and compression loadings is numerically simulated. The constitutive equations presented in Section 2 and in Appendix are implemented in Abaqus 6.11 subroutine UMAT (implicit temporal integration scheme). The matrix material is a fictitious polymer, polyamide (PA) type. Its elastic behaviour follows Hooke's laws for isotropic linear elasticity (23). The Drucker–Prager criterion for plasticity is used (cf Section 2.1 and Appendix). As suggested by Doghri et al. (2011) for a PA6,6, the evolution of the yield stress is given by a linear-exponential hardening law (18), with material parameters given in Table 1. Yet, a different behaviour under compression than under tension is considered here. In particular, initial yield stresses σ_C and σ_T are different (Table 1, $\eta = 0.48$ (4) and $\xi = 1.16$ (5)). In the case of a positive hydrostatic stress, porosities are assumed to developed in the matrix material during the plastic flow and the plastic Poisson coefficient, v_p, is fixed to 0.1. It can be noticed that this value corresponds to experimental results obtained for an other polymer tested in our laboratory (Epee et al., 2011) and is not necessarily representative of the actual behaviour of PA6,6. Yet, this value of v_p allows the analysis of the modelling of a compressible matrix material, given that the numerical tests do not aim at reproducing the real behaviour of PA6,6. It is assumed that porosities can not develop in the matrix material if it is subjected to a compressive loading; v_p is therefore equal to 0.5 for negative hydrostatic stresses (isochoric plastic flow). The parameter γ is computed using the relation (19). All the matrix material parameters are given in Table 1:

$$\sigma_y = \sigma_T + k_1 p + k_2[1 - \exp(-mp)] \quad (18)$$

$$\gamma = \frac{9}{2} \frac{1 - 2v_p}{1 + v_p} \quad (19)$$

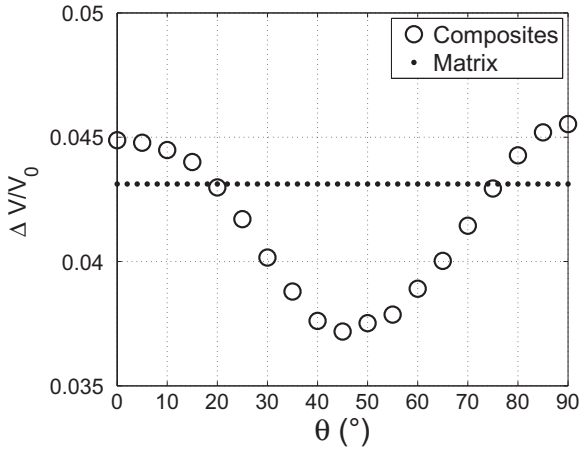

Fig. 6. Relative volume variations of the composite materials – tension.

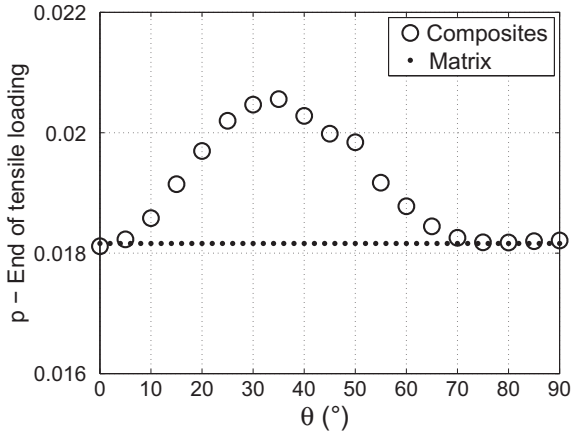

(a) Cumulated plastic strain at the end of the loading

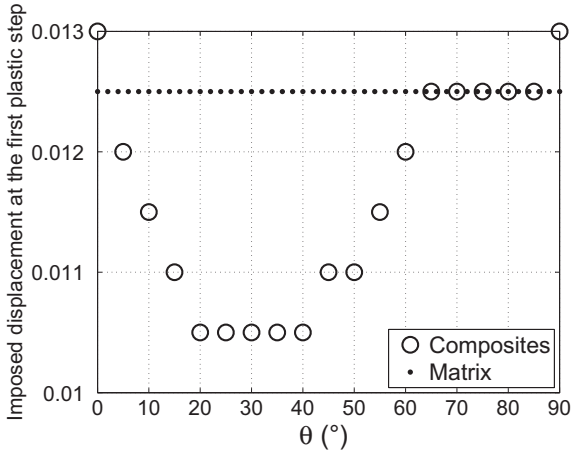

(b) First plastic step

Fig. 7. Influence of the fibres orientation on the matrix plastic flow – tension.

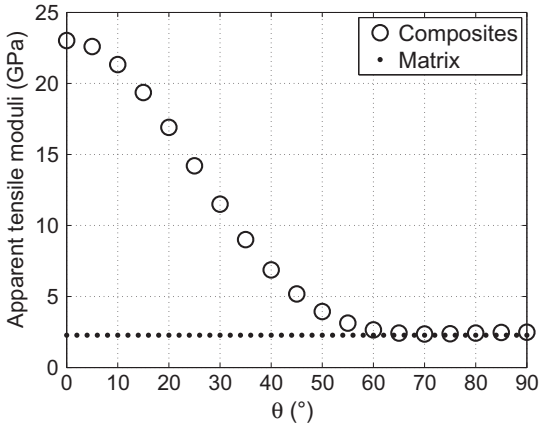

Fig. 8. Influence of the fibres orientation on the composites apparent tensile moduli.

Short fibres have a Young modulus equal to 72 GPa, which is typical of short glass fibres. A total volume fraction of 0.3 is considered for the fibres. They are oriented in the plane $(\vec{x},\vec{z})$, with an angle θ with respect to the axis of loading, $\vec{z}$ (Fig. 1). Different values of θ are tested.

3.1. Tensile tests

The finite element (FE) model of the tensile tests consists of a cube of 1 mm^3, divided into 8 cubic element (C3D8, 8 nodes, full integration). All degrees of freedom are locked at the basis of the cube (i.e., nodes located at $z = 0$). Boundary conditions $u_x = 0$ and $u_y = 0$ are imposed to upper nodes, located at $z = 1$ *mm*, while they are subjected to a total imposed displacement of 5.10^{-2} mm in direction $\vec{z}$ (101 steps, including non-deformed state, constant increment of imposed displacement of 5.10^{-4} mm).

Several composite materials are considered. Each of them is constituted of a unique family of fibres with an angle of orientation, θ, varying from 0° (perfectly aligned fibres) to 90°, by steps of 5°. Fig. 2 shows the levels of axial stress, σ_{zz}, reached in the composites at the end of the tensile loading. In addition, Fig. 3 gives some examples of axial stress time histories computed at the elements centroids. As expected, axial stress levels carried out by the composite with low-angled glass fibres are strongly increased compared to those computed for the neat matrix material, mainly because of the important difference between Young moduli values. When the values of θ increases, the axial stress levels in the composites become logically closer to those of the neat matrix material. For highly angled fibres ($\theta \geqslant 60°$) the differences become negligible and at $\theta = 90°$ the axial stress in the composite equals that of the neat matrix (lower bound assumption).

When fibres are not aligned with axes $\vec{x}$ or $\vec{z}$ (i.e., $\theta \neq 0 + k\frac{\pi}{2}$), shear stress σ_{xz} develops in the composites (fibres are dispersed in the $(\vec{x},\vec{z})$ plane). σ_{xy} and σ_{yz} stay logically null; σ_{yy} remains very low because $\sigma_{F,yy}$ stays null. At the contrary, the presence of fibres greatly influences the values of σ_{xx}. Fig. 4 illustrates these points for the case $\theta = 30°$. The axial strain, ε_{zz}, is identical for all the materials because of the loading conditions. At the contrary, the values of the transverse strains, ε_{xx} and ε_{yy}, that are computed in the composite materials strongly depend on the orientation of the short fibres (Fig. 5 at the end of the tensile loading). As expected, the contraction of the material is homogeneous along directions $\vec{x}$ and $\vec{y}$ in the neat matrix material and for the composite with perfectly aligned glass fibres. It can be seen that the presence of aligned fibres logically lead to a decrease of transverse strains because of the higher rigidity of the composite compared to that of the neat matrix material. When fibres are not aligned with respect to the axis of loading, the strain state becomes totally heterogeneous (i.e., $\varepsilon_{xx} \neq \varepsilon_{yy}$). First, for relatively low angles of orientation, the absolute value of ε_{xx} increases compared to the case of aligned fibres to enable the stretching of angled fibres required to respect the imposed displacement. Then, when fibres orientation becomes closer to axis $\vec{x}$ (i.e., for high values of θ), the fibres strongly act against the deformation in direction $\vec{x}$ and values of ε_{xx} in the composites become lower than that of the neat matrix. As a result of the high Young modulus of the glass fibres the value of ε_{xx} is almost null in the case of transverse fibres (i.e., $\theta = 90°$). The presence of fibres does not directly influence the value of strain component ε_{yy}, since the fibres are distributed in the plane $(\vec{x},\vec{z})$. Nevertheless, this value is adjusted to respect the energy equilibrium during loading.

The relative variation of the material volume, $\frac{\Delta V}{V_0}$, during loading is computed from the trace of the strain tensor (20). As expected, the transformation of the matrix material leads to a volume creation that is also observed for all the composite materials (Fig. 6, at the end of the tensile loading). In accordance with the strain states (Fig. 5), the material expansion is more important in the composites with low-angled fibres. It decreases for intermediate values of the angle of orientation because of the high transverse strains that are computed in these configurations. It becomes again higher than that of the neat matrix in the composites with highly-angled fibres, because of the low values of ε_{xx}:

$$\frac{\Delta V}{V_0} = \exp\left[tr(\bar{\varepsilon})\right] - 1 \tag{20}$$

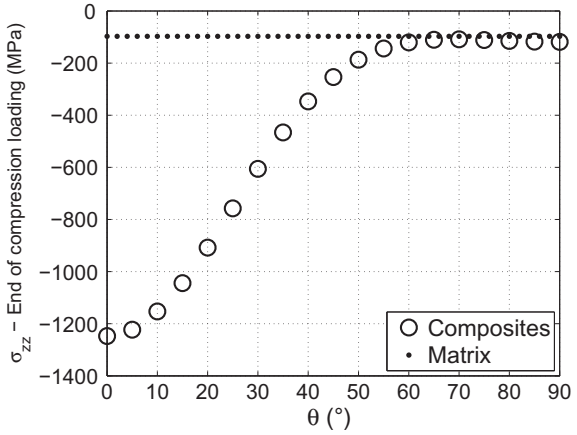

Fig. 9. Composites axial stress at the end of compression loading.

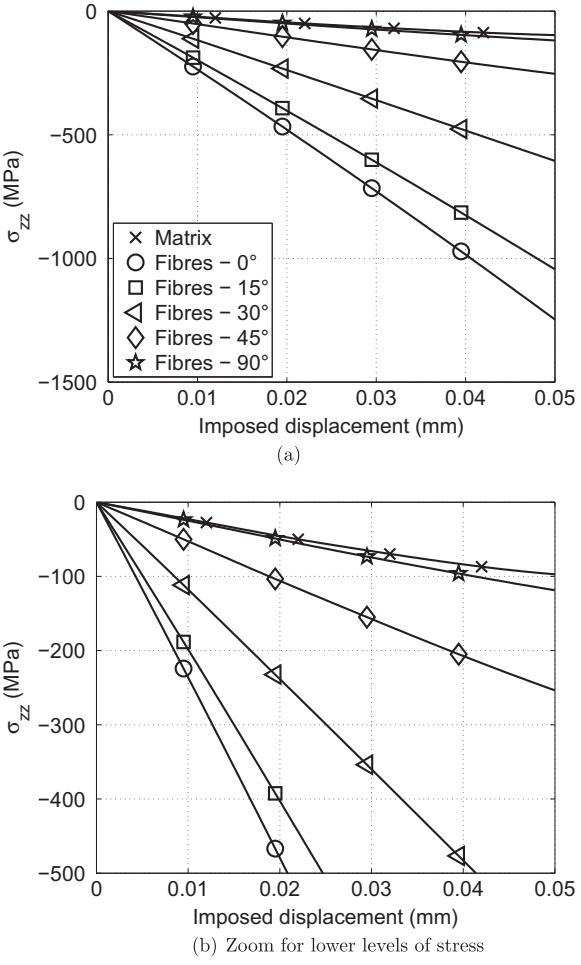

Fig. 10. Axial stresses for different composites PA-30% GF under compression.

where $\Delta V = V - V_0$ with V the current volume and V_0 the initial volume (1 mm^3).

It is reminded that a non isochoric plastic flow is modelled in the matrix material when the material is subjected to a positive hydrostatic stress. With a plastic Poisson coefficient equals to 0.1, the volume variation due to the plastic strain, i.e. $\frac{\Delta V^p}{V_0} = exp[tr(\bar{\varepsilon}^p)] - 1$, represents an important part of the total volume variation. For example, it is responsible of about 65% of the volume variation of the neat matrix material and of about 80% for composites with fibres angles of orientation close to 45°. It is directly linked to the levels of cumulated plastic strain that are reached in the materials. For angles of orientation varying

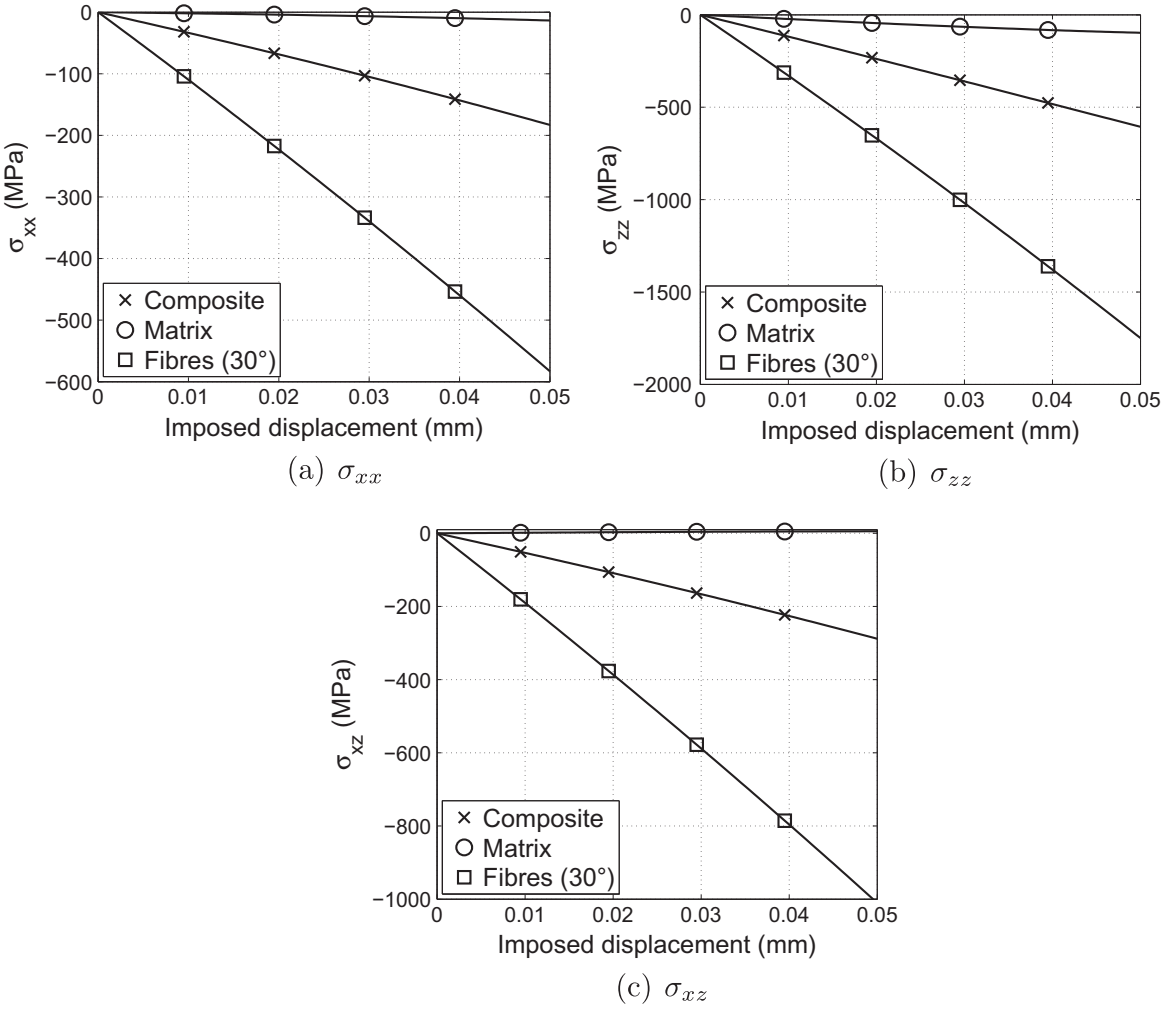

Fig. 11. Stresses under compression for the 30%vol. GF composite, the matrix material and the fibres ($\theta = 30°$).

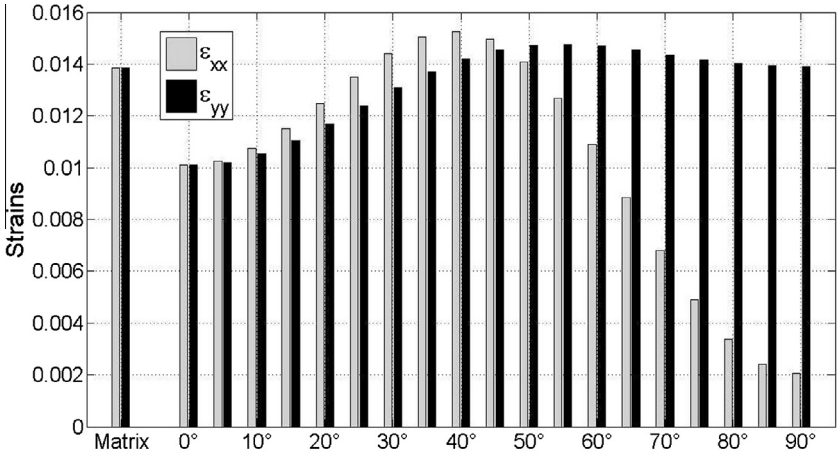

Fig. 12. Transverse strains of the composite materials – compression.

from 10° to 65°, the cumulated plastic strain, p, reaches higher values in the composites than in the neat matrix (Fig. 7(a)) and the plastic flow develops earlier (i.e. for lower values of imposed displacement, Fig. 7(b)). At the contrary, the presence of highly-angled fibres do not fundamentally modify the plastic flow.

Finally, it is interesting to observe the influence of fibres orientation on the rigidity of the composites. The apparent tensile moduli are therefore computed as the ratio between the axial stress, σ_{zz}, and the axial strain, ε_{zz}, at the last elastic step of loading (i.e., the last increment with $p = 0$). In accordance with axial stress levels (Fig. 2), the apparent rigidity of the composite becomes very high when fibres are perfectly aligned (23 GPa against 2.2 GPa for the neat matrix) and then logically decreases when the angle of orientation, θ, increases (Fig. 8). As expected, the rigidities of the composites with highly angled fibres (i.e. $\theta \geqslant 60°$) are very close to that of the neat matrix material.

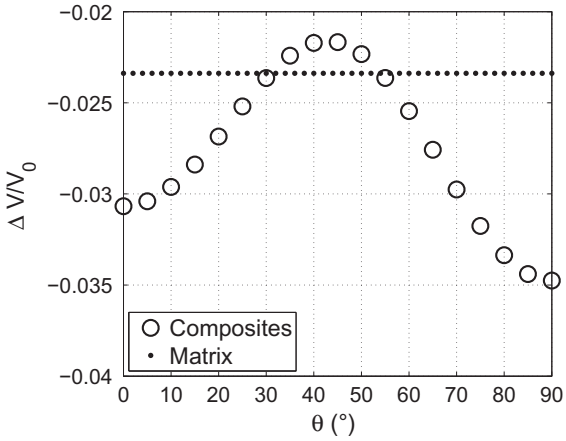

Fig. 13. Relative volume variations of the composite materials – compression.

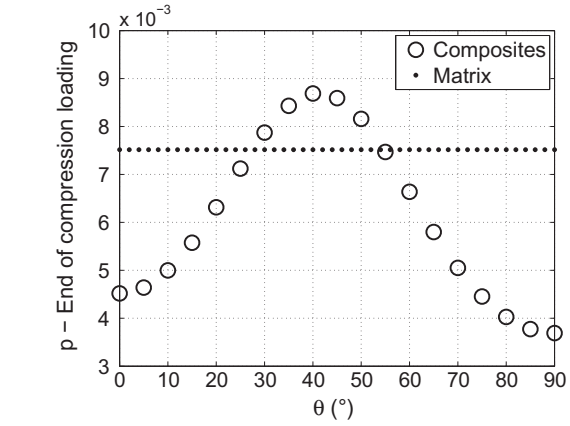

(a) Cumulated plastic strain at the end of the loading

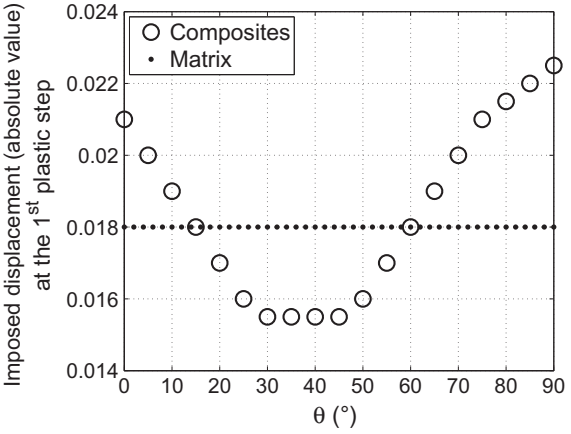

(b) First plastic step

Fig. 14. Influence of fibres orientation on the plastic flow in the matrix – compression.

Table 2
Material parameters of the Al-5,5Mg matrix (Doghri and Tinel, 2005).

Parameter	Value
Young modulus, E_m	70.2 GPa
Poisson coefficient, ν_M	0.33
Initial yield stress, σ_0	100 MPa
Hardening modulus, K	479 MPa
Hardening exponent, n	0.36

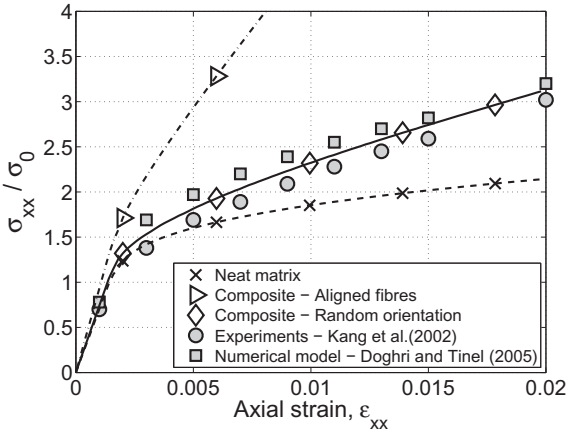

Fig. 15. Tensile behaviour of composite Al-5,5Mg+10%vol. Al_2O_3.

Table 3
Material parameters of the PA6,6 matrix (from Kammoun et al., 2011).

Parameter	Value
Young modulus, E_M	3.1 GPa
Poisson coefficient, ν_M	0.35
Initial yield stress, σ_0	25 MPa
Hardening modulus (linear part), k_1	150 MPa
Hardening modulus (exponential part), k_2	20 MPa
Hardening parameter, m	325

3.2. Compression tests

Compression tests are now simulated using the same FE models as in the previous Section 3.1, except that the upper nodes are now subjected to a total imposed displacement of -5.10^{-2} mm in direction z (101 steps). As in Section 3.1, tests are run for fibres angles of orientation varying from 0° to 90°.

Fig. 9 shows the axial stresses, σ_{zz}, computed at the end of compression loading for the different composites; Fig. 10 gives examples of computed axial stress time histories. Again, the presence of low-angled fibres logically leads to a very important increase of stress levels (in absolute values). This increase is more moderate for angled fibres. For high values of θ the reinforcement becomes ineffective since axial stress levels computed for the composites are similar to those of the neat matrix. The elastic apparent moduli, $\frac{\sigma_{zz}}{\varepsilon_{zz}}$, under compression are the same as those previously computed under tension (Fig. 8).

Table 4
Weight of each fibres angle of orientation with respect to the injection flow direction for the 3 composites PA6,6-GF.

Angle (°)	Weights of angle of orientation		
	10% GF	16% GF	30% GF
0	0.115917	0.161345	0.207872
5	0.103806	0.129412	0.148236
10	0.079585	0.082353	0.080082
15	0.057093	0.050420	0.046004
20	0.041522	0.033613	0.028966
25	0.031142	0.023529	0.018743
30	0.024221	0.016807	0.013631
35	0.019031	0.013445	0.010223
40	0.015571	0.010756	0.008519
45	0.013841	0.008403	0.006815
50	0.010381	0.006723	0.005964
55	0.010381	0.006723	0.005112
60	0.006920	0.005882	0.005112
65	0.006920	0.005882	0.004260
70	0.006920	0.005042	0.003749
75	0.005190	0.005042	0.003408
80	0.005190	0.005042	0.003408
85	0.005190	0.005042	0.003408
90	0.005190	0.005042	0.003408
95	0.005190	0.005042	0.003408
100	0.005190	0.005042	0.003408
105	0.005190	0.005042	0.003408
110	0.005190	0.005042	0.003408
115	0.006920	0.005882	0.003749
120	0.006920	0.006050	0.004260
125	0.008651	0.006723	0.004260
130	0.010381	0.008403	0.005964
135	0.010381	0.009244	0.006815
140	0.015571	0.011765	0.008519
145	0.019031	0.013445	0.010223
150	0.024221	0.016807	0.013631
155	0.031142	0.023529	0.018743
160	0.041522	0.033613	0.028966
165	0.057093	0.052101	0.046004
170	0.079585	0.082353	0.080082
175	0.103806	0.129412	0.148236
Total	1	1	1

The stress and strain states under compression are influenced by the same phenomena previously described for the tensile tests (cf Section 3.1) and their evolution is therefore similar (same conditions of loading). Fig. 11 gives examples of computed stresses for the case $\theta = 30°$. As expected, the presence of angled fibres influences the composite axial stress but also components σ_{xx} and σ_{xz}. σ_{yz} and σ_{xy} remain null. Fig. 12 shows the transverse strains computed at the end of the compression loading for all the materials. Again, the axial strain, ε_{zz}, remains identical for all the materials. The evolutions of the transverse strains follow exactly the same trends than under tension.

The present compression loading leads to a volume reduction of all the composite materials (Fig. 13). It is reminded that the plastic Poisson coefficient is equal to 0.5 for negative hydrostatic stresses. The plastic flow that develops in the matrix material during these compressive tests is therefore isochoric. The volume reduction of the composite materials is generally more important than that of the neat matrix, except for values of θ from 35° to 55°. An explanation is that an earlier development of the plastic flow in these composites (Fig. 14) limits the volume variation, only resulting from the elastic transformation here.

4. Comparisons to experimental data

After the numerical analyses, the following paragraphs aim to validate the implementation by comparing results to experimental data found in the literature. The cases of a metal matrix composite and a polymer matrix composite are successively investigated.

4.1. Al-5,5Mg matrix reinforced with 10%vol. Al_2O_3 short fibres

The behaviour of a composite constituted of an aluminum-magnesium alloy matrix (Al-5,5Mg) reinforced with short fibres of aluminum oxide (Al_2O_3, 10%vol.) and subjected to uniaxial tensile loading is investigated. Experimental data, resulting from works by Kang et al. (2002) and presented by Doghri and Tinel (2005), are taken as references to validate the present implementation.

According to Doghri and Tinel (2005), the matrix behaviour is modelled in J_2-plasticity with a power isotropic hardening law (21), with material parameters listed in Table 2. The fibres have a linear elastic behaviour ($E_F = 300$ GPa). They are randomly oriented in the plane $(\vec{x}, \vec{y})$, with $\vec{x}$ the loading axis:

$$\sigma_y = \sigma_0 + Kp^n \tag{21}$$

The FE model is a simple cube (unique element C3D8), with edges of 1 mm (all coordinates between 0 and 1). Boundary conditions of symmetry are imposed to model the uniaxial test (i.e. $u_x = 0$, $u_y = 0$ and $u_z = 0$ imposed at nodes of coordinate $x = 0$, $y = 0$ and $z = 0$, respectively). A total displacement of 2.10^{-2} mm is imposed along axis $\vec{x}$ to the nodes located at

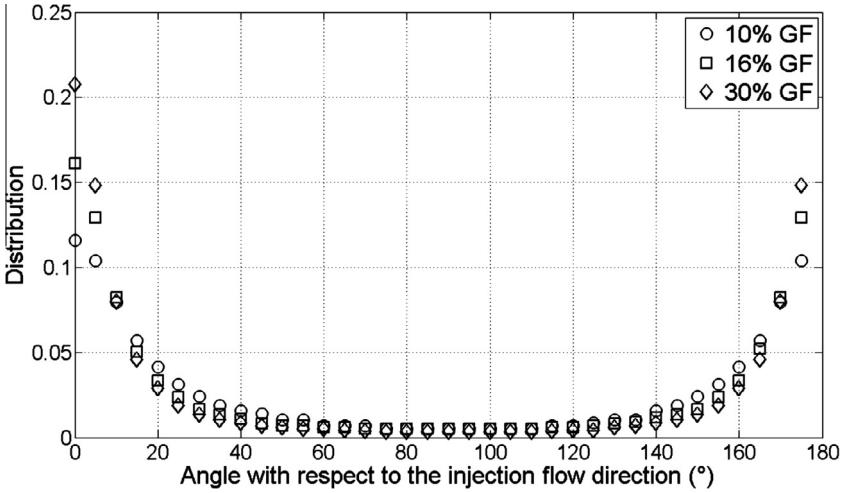

Fig. 16. Distributed orientations of short fibres in the 3 composites PA6,6-GF.

$x = 1$ mm. The simulation is divided into 101 steps, with a constant increment of imposed displacement. To model the random orientation of fibres, the composite material is constituted of 10 families of fibres, each of them representing 1% of the total volume, with angles of orientation varying from 0° to 90°, by step of 10°.

Fig. 15 allows to compare the axial stresses computed with the current model to the experimental data of Kang et al. (2002). For comparative purposes, the axial stresses computed for the case of perfectly aligned fibres are also shown. As expected, they are over-estimated. However, the computation that model a random in-plane orientation for the fibres leads to stress levels close to experimental data. Results of the present implementation can also be compared to those obtained by Doghri and Tinel (2005) with a two-step procedure of homogenisation (Fig. 15). It can be seen that both numerical implementations lead to similar gaps with experimental data. So, the tensile behaviour of materials reinforced with randomly oriented short fibres can be modelled satisfactorily with the present implementation like with complex two-step procedures of homogenisation.

4.2. PA6,6 matrix reinforced with short glass fibres

Kammoun et al. (2011) present the tensile behaviours of composites constituted of a polyamide PA6,6 matrix reinforced with

Table 5
Volume fractions of each short-glass-fibres family for the 3 composites PA6,6-GF.

Angles in the material subroutine	Added contributions	Fibres' volume fraction		
		10% GF	16% GF	30% GF
θ	$\theta + \{0°, 5°, 175°, 180°\}$	0.032353	0.067227	0.130857
$\theta + 10°$	$\theta + \{10°, 15°, 165°, 170°\}$	0.027336	0.042756	0.090987
$\theta + 20°$	$\theta + \{20°, 25°, 155°, 160°\}$	0.014533	0.018286	0.032203
$\theta + 30°$	$\theta + \{30°, 35°, 145°, 150°\}$	0.008651	0.009681	0.015335
$\theta + 40°$	$\theta + \{40°, 45°, 135°, 140°\}$	0.005536	0.006427	0.009456
$\theta + 50°$	$\theta + \{50°, 55°, 125°, 130°\}$	0.003979	0.004571	0.006901
$\theta + 60°$	$\theta + \{60°, 65°, 115°, 120°\}$	0.002768	0.003792	0.004958
$\theta + 70°$	$\theta + \{70°, 75°, 105°, 110°\}$	0.002249	0.003227	0.004192
$\theta + 80°$	$\theta + \{80°, 85°, 95°, 100°\}$	0.002076	0.003227	0.004089
$\theta + 90°$	$\theta + 90°$	0.000519	0.000807	0.001022
	Total	0.1	0.16	0.3

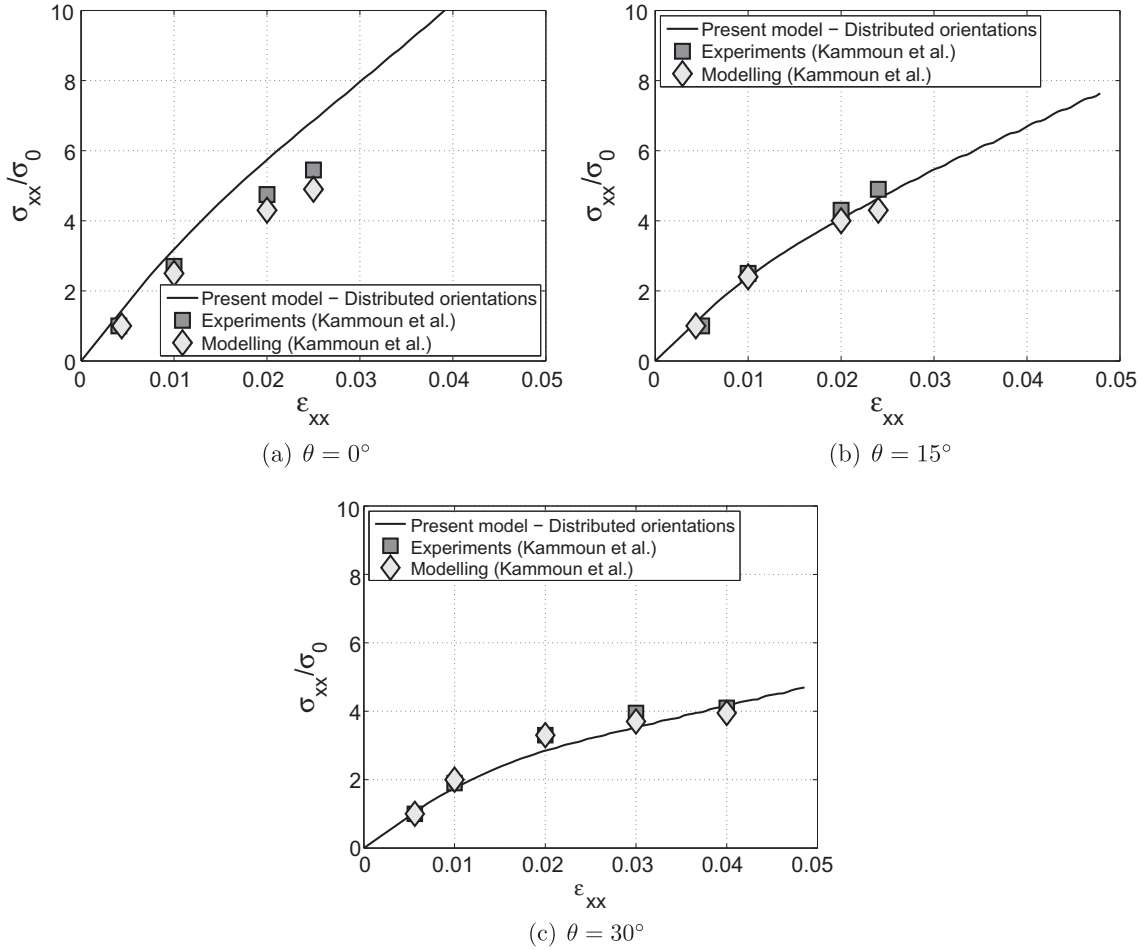

Fig. 17. Tensile behaviours of composite PA6,6+10%vol. glass fibres.

short glass fibres ($v_f = 10\%$, 16% and 30%). According to Kammoun et al. (2011), the matrix behaviour is modelled in J_2-plasticity with a linear exponential isotropic hardening law (18). The initial yield stress is not given in the article (Kammoun et al., 2011), as it is a confidential parameter. Consequently, a value of 25 MPa is chosen as a typical value for polyamides. Material parameters of the PA6,6 matrix are listed in Table 3. Glass fibres have a linear elastic behaviour ($E_F = 76$ GPa).

The tensile specimens are cut in injection molded sheets at different angles, θ, varying from 0° to 90° with respect to the injection flow direction. The fibres are mainly oriented along the injection flow direction but not perfectly, as studied in detail by Kammoun et al. (2011) and Doghri and Tinel (2006), in particular. So, the modelling of the different tensile loadings in the present implementation must consider a distribution of fibres' angles of orientation around θ instead of a unique orientation. This distribution is computed following the works of Doghri and Tinel (2006) for fibres' angles of orientation varying from 0° to 180° with respect to the injection flow direction. Results are given in Table 4 in terms of weight to be associated to each angle (cf also Fig. 16). It can be seen that the distribution depends on the total volume fraction of the fibres: the higher the density of fibres, the more they tend to orient in the injection flow direction.

As in Section 4.1, the FE model is a cube of 1 mm-edges (1 element C3D8), subjected to the same boundary conditions. A total displacement of 5.10^{-2} mm is imposed. The distribution of fibres is modelled in a simple way. The composite material is constituted of 10 families of fibres with angles of orientation varying from θ to $\theta + 90°$, by step of 10°. As already mentioned, θ stands for the angle between the direction of the tensile loading and the injection flow direction. The volume fractions that must be attributed to each family of fibres is computed using data from Table 4 and are given in Table 5. Angles of orientation $\theta + \alpha$ and $180° - (\theta + \alpha)$, $\forall \alpha \in [0; 90°]$, are associated. It is justified because they lead to the computation of the same axial stresses, since the diagonal terms in the matrix of orientation, A, are obviously the same for angles $\theta + \alpha$ and $180° - (\theta + \alpha)$.

Figs. 17–19 show the results of the implementation for the composites with a volume fraction of 10%, 16% and 30% fibres, respectively, and for angles of loading of $\theta = 0°$, 15° and 30° with respect to the injection flow direction. Results can be compared to the experimental and numerical data provided by Kammoun et al. (2011). It must be pointed out that these comparisons may be biased by the uncertainties concerning the real value of the matrix initial yield stress.

For all composites, computed axial stresses are overestimated when the loading is applied in the injection flow direction (i.e., $\theta = 0°$), with gaps increasing when increasing the fibre content. Yet, computed results match well the experimental data for $\theta = 15°$ and 30°. For the highest fibre contents, gaps increase at the end of loadings. In particular, the inflexion of the experimental stress vs. strain curve is not modelled. It can be explained by a softening of the matrix material due to damage and/or fibres progressive debonding that are not considered in the current model.

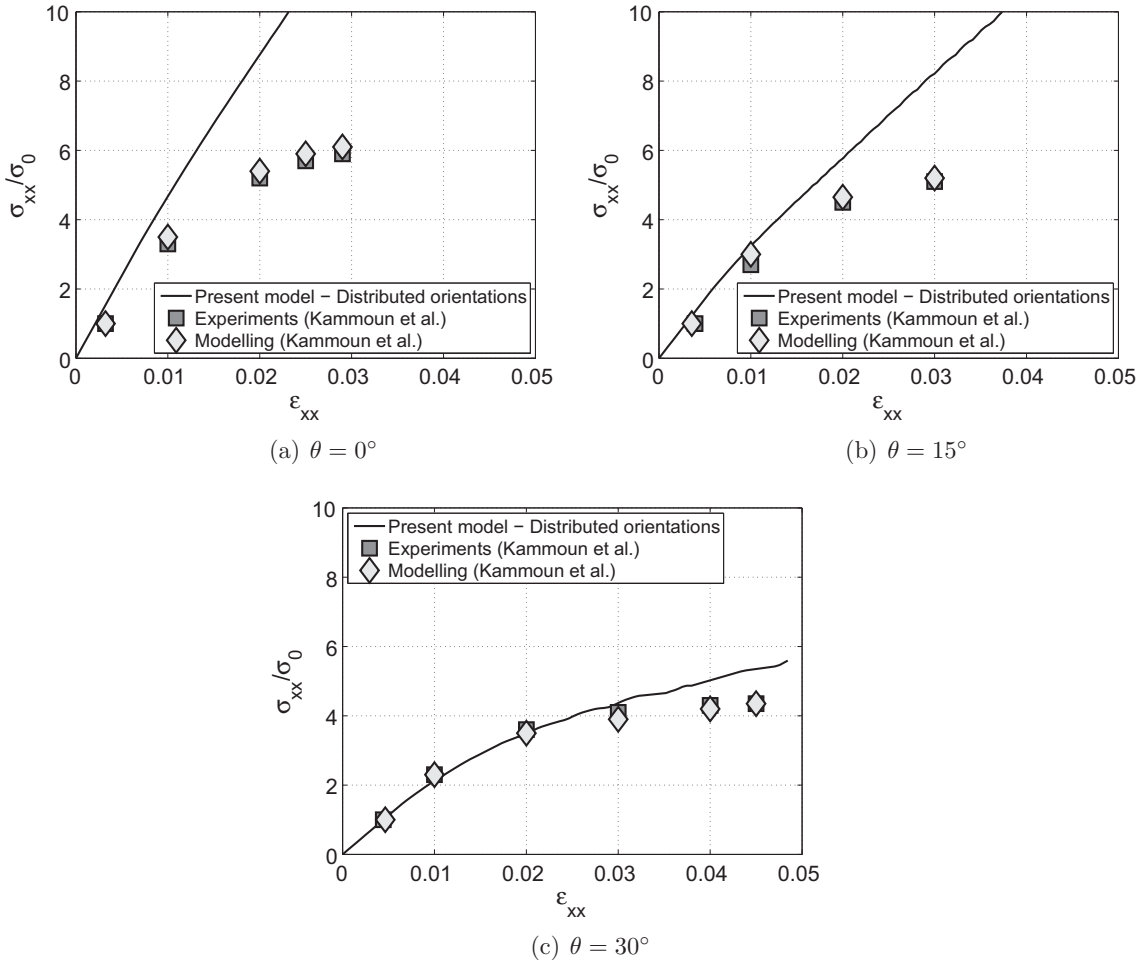

Fig. 18. Tensile behaviours of composite PA6,6+16%vol. glass fibres.

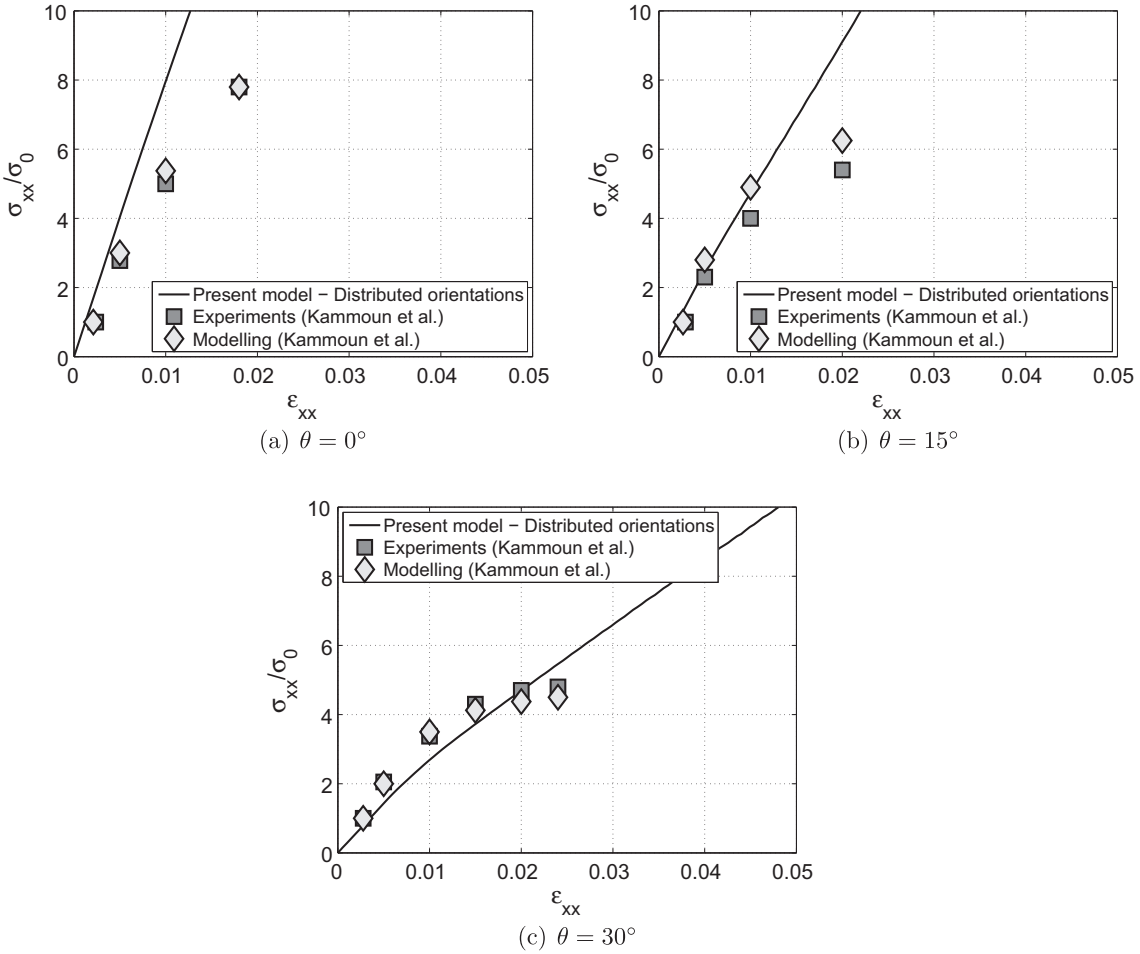

(a) $\theta = 0°$ (b) $\theta = 15°$

(c) $\theta = 30°$

Fig. 19. Tensile behaviours of composite PA6,6+30%vol. glass fibres.

5. Conclusion

This paper presents an efficient modelling of the mechanical behaviour of short fibre reinforced composite materials. The composite material is seen as an assembly of a matrix medium and of several fibre media, linked by a multiplicative decomposition of the deformation gradient that applies to the whole composite. Each fibre medium is characterised by a unique direction of orientation and is assumed to have a one-dimensional linear elastic behaviour in this direction. The 3-dimensional elastoplastic behaviour of the matrix is modelled using the Drucker–Prager criterion for plasticity and non-associative plasticity rules so that compressible media can be dealt with. It can be of great importance when dealing with polymer matrix composites, in particular. The behaviours of the matrix and the families of fibres are obtained separately. Then, the 3-dimensional fully anisotropic behaviour of the composite is computed assuming an additive decomposition of the plastic potential.

The influence of the orientation of the short fibres on the mechanical fields computed during numerically simulated tensile and compression tests is investigated in detail. The analyses reveal that the presence of angled fibres with respect to the loading axis logically affects the strain and stress states of the composites but also influences the development of the plastic flow in the matrix material and the material volume variation.

Comparisons between experimental data found in the literature prove that the present implementation can predict the tensile behaviours of metal and polymer matrix composites. In particular, random orientations or imperfect alignments of the short fibres can be modelled in a very simple way, without needing complex procedures such as two-step homogenisation schemes. However, axial stresses computed for perfectly aligned reinforcements seem to be overestimated.

Further developments concern first the modelling of the matrix damage and possibly the extension of the model to rate-dependent material behaviours (viscoelasticity, viscoplasticity,...). An interesting issue that needs more thorough work is to model a progressive debonding and/or an imperfect load transmission at the matrix/fibres interfaces since that can have a significant influence on the macroscopic properties of the composite material.

Acknowledgements

The present research work has been supported by International Campus on Safety and Intermodality in Transportation, the Nord-Pas-de-Calais Region, the European Community, the Regional Delegation for Research and Technology, the Ministry of Higher Education and Research and the National Center for Scientific Research. The authors gratefully acknowledge the support of these institutions.

Appendix A. Implementation of the matrix material behaviour

Under the hypothesis of small deformations, the strain tensor, $\bar{\varepsilon}$, that is applied to the matrix material is split into a reversible (elastic) part, $\bar{\varepsilon}^e$, and an irreversible (plastic) one, $\bar{\varepsilon}^p$, so that $\bar{\varepsilon} = \bar{\varepsilon}^e + \bar{\varepsilon}^p$.

The plastic strain tensor is used to compute the cumulated plastic strain (22).

$$p = \int \sqrt{\frac{2}{3}\dot{\bar{\varepsilon}}^p : \dot{\bar{\varepsilon}}^p}dt \tag{22}$$

The isotropic elastic behaviour of the matrix is modelled by Hooke's linear laws. Lamé's relation (23) is then used to express the Cauchy stress tensor for the matrix, $\bar{\sigma}_M$, from the elastic strain tensor.

$$\bar{\sigma}_M = 2\mu_M\bar{\varepsilon} + \Lambda_M tr(\bar{\varepsilon}) \tag{23}$$

The Lamé coefficients, μ_M and Λ_M, are related to the more commonly encountered parameters E_M (Young modulus) and ν_M (Poisson coefficient) since $\mu_M = \frac{E_M}{1+\nu_M}$ and $\Lambda_M = \frac{\nu_M E_M}{(1+\nu_M)(1-2\nu_M)}$. From now on, the subscript M will be omitted to simplify the notations.

As stated in the core of the article, the pressure sensitive criterion of Drucker–Prager is used to describe the plastic flow (2) and a parameter ξ is introduced in the expression of the yield surface (3) to model a different yield stress in tension (σ_T) than in compression ($\sigma_C < 0$). Material parameters η and ξ can be expressed from σ_T and σ_C by considering uniaxial tensile and compressive tests leading to one-dimensional stress states. Under tension, the plastic flow begins as soon as $\sigma_T + \frac{\eta}{3}\sigma_T = \xi\sigma_T$ and under compression as soon as $-\sigma_C + \frac{\eta}{3}\sigma_C = \xi\sigma_T$ ($\sigma_C < 0$). It immediately gives rise to the expressions (4) and (5) for η and ξ, respectively. It is reminded that the framework of non associative plasticity is considered, with a pressure sensitive plastic potential (7).

The implementation of these constitutive laws is adapted from the classical scheme of return-mapping algorithm, developed for J_2-plasticity by Simo and Hughes (1998). Mechanical quantities are computed at increment $n+1$ from quantities at increment n following an implicit scheme for temporal integration. In the preamble of the implementation, a subroutine is used to build a table that links the values of the cumulated plastic strain to those of the yield stress, according to the hardening law. In practice, a piecewise linear approximation of the hardening law is assumed on each interval of cumulated plastic strain $[p_i; p_{i+1}[$, with $p_0 = 0$ and $p_{i+1} = p_i + 10^{-4}\ \forall i$ (24):

$$\sigma_y^{tr} = \sigma_{y\ i} + (p^{tr} - p_i)\underbrace{\frac{\sigma_{y\ i+1} - \sigma_{y\ i}}{p_{i+1} - p_i}}_{=K} \text{ if } p^{tr} \in [p_i; p_{i+1}[\tag{24}$$

where $\sigma_{y\ i}$ and $\sigma_{y\ i+1}$ are the exact values of the yield stress computed at $p = p_i$ and $p = p_{i+1}$, respectively, i.e. $\sigma_{y\ i} = \sigma_T + R(p_i)$ (6).

The first step of elastic prediction assumes an elastic evolution between increment n and $n+1$. A "trial" state is therefore defined (25) assuming that all the strain increment is elastic. The deviatoric part of the trial stress, $\bar{S}^{tr}$, and the trial hydrostatic pressure, σ_H^{tr}, are obviously computed from $\bar{\sigma}^{tr}$. The trial yield stress, σ_y^{tr}, is found according to the piecewise approximation of the hardening law (24) around the value of p^{tr} (previously described subroutine). Finally, the trial yield surface, f^{tr}, can be expressed (26):

$$\begin{cases} \bar{\varepsilon}_{n+1} = \bar{\varepsilon}^e_{n+1} + \bar{\varepsilon}^p_{n+1} = \bar{\varepsilon}_n + \Delta\bar{\varepsilon} \\ \bar{\varepsilon}^{e\ tr} = \bar{\varepsilon}^e_n + \Delta\bar{\varepsilon} \\ \bar{\varepsilon}^{p\ tr} = \bar{\varepsilon}^p_n \\ p^{tr} = p_n \\ \bar{\sigma}^{tr} = 2\mu\bar{\varepsilon}^{e\ tr} + \Lambda tr(\bar{\varepsilon}^{e\ tr}) \end{cases} \tag{25}$$

$$f^{tr} = J_2^{tr} + \eta\sigma_H^{tr} - \xi\sigma_y^{tr} \tag{26}$$

If $f^{tr} < 0$, the material evolution is actually elastic between increments n and $n+1$ and the actual mechanical quantities are equal to trial ones (25). If not, a plastic correction is needed since plastic flow occurred.

The normality rule (27) expresses the evolution of the plastic strain by introducing a plastic multiplier, λ. The expression is discretized for an implicit scheme (28) taking the definition (7) of the plastic potential into account. The increment of cumulated plastic strain is then expressed from $\Delta p = \sqrt{\frac{2}{3}\Delta\bar{\varepsilon}^p : \Delta\bar{\varepsilon}^p}$, noting that $\bar{S}_{n+1} : \bar{S}_{n+1} = \frac{2}{3}J^2_{2,n+1}$ and $\bar{S}_{n+1} : \bar{I} = tr(\bar{S}_{n+1}) = 0$ (29):

$$\dot{\bar{\varepsilon}}^p = \dot{\lambda}\frac{\partial\psi}{\partial\bar{\sigma}} \tag{27}$$

$$\Delta\bar{\varepsilon}^p = \Delta\lambda\left(\frac{3}{2}\frac{\bar{S}_{n+1}}{J_{2,n+1}} + \frac{\gamma}{3}\bar{I}\right) \tag{28}$$

with $\bar{I}$ the 3×3 identity matrix:

$$\Delta p = \Delta\lambda\sqrt{1 + \frac{2}{9}\gamma^2} \tag{29}$$

Injecting the relation (28) into the expression (25) of $\bar{\sigma}^{tr}$ gives the expressions (30) for the actual stress tensor, (31) for the hydrostatic pressure and (32) for the stress deviator:

$$\begin{aligned} \bar{\sigma}_{n+1} &= \bar{\sigma}^{tr} - 2\mu\Delta\bar{\varepsilon}^p - \Lambda tr(\Delta\bar{\varepsilon}^p)\bar{I} \\ &= \bar{\sigma}^{tr} - 2\mu\Delta\lambda\left(\frac{3}{2}\frac{\bar{S}_{n+1}}{J_{2,n+1}} + \frac{\gamma}{3}\bar{I}\right) - \Lambda\Delta\lambda\gamma\bar{I} \end{aligned} \tag{30}$$

$$\sigma_{H,n+1} = \sigma_H^{tr} - \Delta\lambda\gamma\left(\frac{2}{3}\mu + \Lambda\right) \tag{31}$$

$$\begin{aligned} \bar{S}_{n+1} &= \bar{S}^{tr} - 2\mu\Delta\lambda\frac{3}{2}\frac{\bar{S}_{n+1}}{J_{2,n+1}} \\ &\quad - \underbrace{\left[\frac{2}{3}\mu\Delta\lambda\gamma + \Lambda\Delta\lambda\gamma - \frac{2}{3}\mu\Delta\lambda\gamma - \Delta\lambda\gamma\Lambda\right]}_{=0}\bar{I} \\ &\Rightarrow \bar{S}_{n+1} = \left[1 + 3\mu\frac{\Delta\lambda}{J_{2,n+1}}\right]^{-1}\bar{S}^{tr} \end{aligned} \tag{32}$$

$J_{2,n+1} = \sqrt{\frac{3}{2}\bar{S}_{n+1} : \bar{S}_{n+1}}$ is computed using the relation (32):

$$J_{2,n+1} = J_2^{tr} - 3\mu\Delta\lambda \tag{33}$$

The current yield surface, f_{n+1}, is expressed by relation (34) where the current yield stress, $\sigma_{y,n+1}$, is approximated following the piecewise linear hardening law (35).

$$f_{n+1} = J_{2,n+1} + \eta\sigma_{H,n+1} - \xi\sigma_{y,n+1} = 0 \tag{34}$$

$$\sigma_{y,n+1} = \sigma_{y\ i} + K(p^{tr} + \Delta p - p_i) \tag{35}$$

Finally, the difference between trial and actual yield surfaces gives rise to the expression (36) of the plastic multiplier, λ. It is computed using an iterative Newton scheme. Initial values of K and γ are those computed for p^{tr} and are updated throughout the iterative resolution. The iterative scheme stops as soon as the actual yield surface (34) is computed below a user-defined tolerance value (10^{-4} here). Mechanical quantities for increment $n+1$ are then updated using previous equations with the final value of $\Delta\lambda$.

$$\begin{aligned} f^{tr} - f_{n+1} = f^{tr} &= J_2^{tr} - J_{2,n+1} + \eta(\sigma_H^{tr} - \sigma_{H,n+1}) + \xi K\Delta p \Rightarrow f^{tr} \\ &= 3\mu\Delta\lambda + \eta\Delta\lambda\gamma\left(\frac{2}{3}\mu + \Lambda\right) + \xi K\sqrt{1 + \frac{2}{9}\gamma^2}\Delta\lambda \Rightarrow \Delta\lambda \\ &= \frac{f^{tr}}{3\mu + \eta\gamma\left(\frac{2}{3}\mu + \Lambda\right) + \xi K\sqrt{1 + \frac{2}{9}\gamma^2}} \end{aligned} \tag{36}$$

References

Bernasconi, A., Cosmi, F., Dreossi, D., 2008. Local anisotropy analysis of injection moulded fibre reinforced polymer composites. Compos. Sci. Technol. 68, 2574–2581.

Bernasconi, A., Cosmi, F., 2011. Analysis of the dependence of the tensile behaviour of a short fibre reinforced polyamide upon fibre volume fraction, length and orientation. Procedia Eng. 10, 2129–2134.

Böhm, H.J., Eckschlager, A., Han, W., 2002. Multi-inclusion unit cell models for metal matrix composites with randomly discontinuous reinforcements. Comput. Mater. Sci. 25, 42–53.

Bowyer, W.H., Bader, M.G., 1972. On the re-inforcement of thermoplastics by imperfectly aligned discontinuous fibres. J. Mater. Sci. 25, 42–53.

Detassis, M., Pegoretti, A., Migliaresi, C., 1995. Effect of temperature and strain rate on interfacial shear stress transfer in carbon/epoxy model composites. Compos. Sci. Technol. 53, 39–46.

Doghri, I., Ouaar, A., 2003. Homogenization of two-phase elasto-plastic composite materials and structures. Study of tangent operators, cyclic plasticity and numerical algorithms. Int. J. Solids Struct. 40, 1681–1712.

Doghri, I., Tinel, L., 2005. Micromechanical modeling and computation of elasto-plastic materials reinforced with distributed-orientation fibers. Int. J. Plast. 21, 1919–1940.

Doghri, I., Tinel, L., 2006. Micromechanics of inelastic composites with misaligned inclusions: numerical treatment of orientation. Comput. Methods Appl. Mech. Eng. 195, 1387–1406.

Doghri, I., Brassart, L., Adam, L., Gérard, J.-S., 2011. A second-moment incremental formulation for the mean-field homogenization of elasto-plastic composites. Int. J. Plast. 27, 352–371.

Drozdov, A.D., Al-Mulla, A., Gupta, R.K., 2003. The viscoelastic and viscoplastic behavior of polymer composites: polycarbonate reinforced with short glass fibers. Comput. Mater. Sci. 28, 16–30.

Drozdov, A.D., Al-Mulla, A., Gupta, R.K., 2005. Finite viscoplasticity of polycarbonate reinforced with short glass fibers. Mech. Mater. 37, 473–491.

Epee, A.F., Lauro, F., Bennani, B., Bourel, B., 2011. Constitutive model for a semi-crystalline polymer under dynamic loading. Int. J. Solids Struct. 48, 1590–1599.

Eshelby, J.D., 1957. The determination of the elastic field of an ellipsoidal inclusion and related problems. Proc. R. Soc. Lond. A241, 376–396.

Facca, A.G., Kortschot, M.T., Yan, N., 2007. Predicting the tensile strength of natural fibre reinforced thermoplastics. Compos. Sci. Technol. 67, 2454–2466.

Fu, S.-Y., Lauke, B., 1996. Effects of fiber length and fiber orientation distributions on the tensile strength of short-fiber-reinforced polymers. Compos. Sci. Technol. 56, 1179–1190.

Hill, R., 1965. Continuum micro-mechanisms of elastoplastic polycrystals. J. Mech. Phys. Solids 13, 89–101.

Kammoun, S., Doghri, I., Adam, L., Robert, G., Delannay, L., 2011. First pseudo-grain failure model for inelastic composites with misaligned short fibers. Compos. Part A 42, 1892–1902.

Kang, G.-Z., Yang, C., Zhang, J.-X., 2002. Tensile properties of randomly oriented short δAl_2O_3 fiber reinforced aluminum alloy composites. I: Microstructure characteristics, fracture mechanisms and strength prediction. Compos. Part A 33, 647–656.

Klinkel, S., Sansour, C., Wagner, W., 2005. An anisotropic fibre-matrix material model at finite elastic–plastic strains. Comput. Mech. 35, 409–417.

Lagoudas, D.C., Gavazzi, A.C., Nigam, H., 1991. Elastoplastic behaviour of metal matrix composites based on incremental plasticity and the Mori–Tanaka averaging scheme. Comput. Mech. 8, 193–203.

Lebensohn, R., Tomé, C., 1993. A self-consistent anisotropic approach for the simulation of plastic deformation and texture development of polycrystals: application to zirconium alloys. Acta Metall. Mater. 41, 2611–2624.

Levy, A., Papazian, J.M., 1991. Elastoplastic finite element analysis of short-fiber-reinforced SiC/Al composites. Effects of thermal treatment. Acta Metall. Mater. 39, 2255–2266.

Lorca, J.L., Needleman, A., Suresh, S., 1991. An analysis of the effect of matrix void growth on deformation and ductility in metal ceramic composites. Acta Metall. Mater. 39, 2317–2355.

Mercier, S., Molinari, A., 2009. Homogenization of elastic-viscoplastic heterogeneous materials: self-consistent and Mori–Tanaka schemes. Int. J. Plast. 25, 1024–1048.

Modniks, J., Joffe, R., Andersons, J., 2011. Model of the mechanical response of short flax fiber reinforced polymer matrix composites. Procedia Eng. 10, 2016–2021.

Mori, T., Tanaka, K., 1973. Average stress in matrix and average elastic energy of materials with misfitting inclusions. Acta Metall. 21, 571–574.

Nedjar, B., 2007. An anisotropic viscoelastic fibre-matrix model at finite strains: continuum formulation and computational aspects. Comput. Methods Appl. Mech. Eng. 196, 1745–1756.

Ponte-Castañeda, P., 2002. Second-order homogenization estimates for nonlinear composites incorporating field fluctuations. 1: Theory. J. Mech. Phys. Solids 50, 737–757.

Schjdt-Thomsen, B., Pyrz, R., 2001. The Mori–Tanaka stiffness tensor: diagonal symmetry, complex fibre orientations and non-dilute volume fractions. Mech. Mater. 33, 531–544.

Simo, J.C., Hughes, T.J.R., 1998. Computational Inelasticity, . Interdisciplinary Applied Mechanics, second ed., vol. 7. Springer, Berlin.

Thomason, J.L., 2001. Micromechanical parameters from macromechanical measurements on glass reinforced polyamide 6,6. Compos. Sci. Technol. 61, 2007–2016.

Thomason, J.L., 2002. Interfacial strength in thermoplastic composites – at last an industry friendly measurement method? Compos. Part A 33, 1283–1288.

Vincent, M., Devillers, E., Agassant, J.-F., 1997. Fibre orientation calculation in injection moulding of reinforced thermoplastics. J. Non-Newtonian Fluid Mech. 73, 317–326.